Journal of Applied Polymer Science

Influence of Different Concentrations of Glycidylisobutyl-POSS on the Glass Transition of Cured Epoxy Resin

Vinicios Pistor,[1] Lucas Puziski,[2] Ademir J. Zattera[2]

[1]Institute of Chemistry, Universidade Federal do Rio Grande do Sul, Porto Alegre, RS, Brazil

[2]Center of Exact Sciences and Technology, LPOL/Universidade de Caxias do Sul, Caxias do Sul, RS, Brazil

Correspondence to: V. Pistor (E-mail: pistorv@yahoo.com.br) and A. J. Zattera (E-mail: ajzattera@terra.com.br)

ABSTRACT: In this study, polyhedral oligomeric silsesquioxane glycidylisobutyl-POSS was dispersed in epoxy resin by ultrasound, and the parameters of a phantom model, the Williams–Landel–Ferry (WLF) and Vogel–Fulcher–Tammann (VFT) equations were modeled using dynamic mechanical analysis (DMA) to evaluate their influence on the glass transition state. The relaxation and retardation time distributions were estimated using a nonlinear regularization method, and the estimated physical parameters were discussed based on the results obtained from transmission electron microscopy (TEM). The TEM analysis indicated higher POSS dispersion with a spherical shape. The POSS dispersion was associated with the formation of micelles due to their hybrid character. The micelles favored the interconnections of the nodular microstructure of the epoxy thermosetting, which led to an increase in their T_g values. These interconnections increased the structure's percolation, promoted a reduction in the thermal expansion coefficient and resulted in a more homogeneous glass transition, in terms of a cooperative distribution in the relaxation times at the time scale measured. © 2014 Wiley Periodicals, Inc. J. Appl. Polym. Sci. **2015**, *132*, 41453.

KEYWORDS: glass transition; nanostructured polymers; resins; structure–property relations; thermal properties

Received 1 June 2014; accepted 25 August 2014

DOI: 10.1002/app.41453

INTRODUCTION

Using advanced nanotechnology, many researchers are studying polyhedral oligomeric silsesquioxane (POSS) dispersed in thermosetting epoxy resin.[1–7] POSS consists of hybrid monomers composed of atoms of silicon (Si) and oxygen (O) in a cage format with octahedral geometry and a size of ≈ 1.5nm.[3] The advantage of POSS lies in the possibility of binding different organic groups to the Si atoms at the cage's vertices. These organic groups generate the hybrid character in the inorganic cage. Moreover, hydroxyl (OH),[1] oxyrane (C_2H_4O)[3] or amine (R—NH, R—NH_2)[6,7] groups act as functional groups at the cage vertices, which can be points of chemical interaction with the epoxy resin. The presence of one of these particular different organic groups is reflected in changes to the glass transition, which is a critical physical property for characterizing thermosetting.[8] Research using POSS containing amine groups reports increases in T_g,[6,7] whereas POSS containing oxyrane groups generally leads to decreases.[3,5] This difference is most likely due to the fact that amine groups are more reactive with epoxy resin than oxyrane groups are with the hardener generally used in epoxy-cured systems. However, the differences in the physical interaction of POSS with cured epoxy resins are numerous. First, it is necessary to consider that the curing of epoxy resin, even with stoichiometry proportions, is an inhomogeneous process.[6–9] The inhomogeneity network is a result of diffusion restriction that occurs during the increase in viscosity when the crosslink network is formed[8] and as a result of the formation of a number of network imperfections, such as intrachain loops.[10] In other words, the thermosetting system presents fluctuations in the crosslink densities that are inherent to stoichiometry.[9] When considering the addition of nanoparticles, their spatial presence (domain size, distribution, dispersion, aspect ratio and shape) or interfacial interaction (physical or chemical) with the matrix are important aspects that may be correlated with the various observed T_g responses.

The glass transition is a complex phenomenon that correlates changes in the energetic level of a molecular vibration with the microstructure of a material.[11] T_g is not a first order transition and is characterized by finite variations in the thermal expansion and thermal capacity. Adam and Gibbs[12] state that the manifestation of this second order transition is dependent on the density of potential energy fluctuations. Discontinuous structures are associated with crystal interfaces, coiled amorphous chains, nodular interfaces or any interface or atomic discontinuity involving anywhere between scales associated with few atoms to the macroscopic. In a glass transition, these

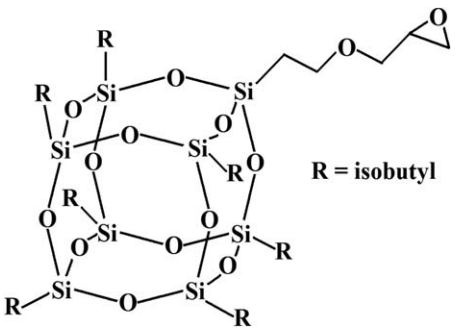

Figure 1. Chemical structure of the glycidylisobutyl—POSS used to obtaining the nanocomposites.

imperfections may be considered cooperative rearrangement regions (CRR),[5–7] and in this case,the thermal fluctuations in the second order transitions may be the key to the modification of this polymer class. Recent studies indicate that POSS can minimize the thermal fluctuations on the nodular interface of epoxy resin due to their ability to form chemical interactions.[5–7] The use of octafunctional POSS with oxyrane[5] and amine groups[6,7] demonstrates different T_g responses; however, dispersion is observed in each case. In this work, nanocomposites containing monofunctional glycidylisobutyl—POSS were manufactured by ultrasound with the goal of evaluating the influence of dispersion on the homogeneity of the epoxy resin microstructure through glass transition theory.

MATERIALS

The epoxy resin diglycidyl ether of bisphenol-A (DGEBA) (Araldite® GY 260) was used in this study with an epoxy equivalent of 5.32–5.44 eq kg^{-1}, and a curing agent based on a cycloaliphatic amine (AradurTM 2963) with an amine equivalent of 5.80–6.20 eq kg^{-1} was used and supplied by Hustman Advanced Materials. The monofunctional polyhedral oligomeric silsesquioxane glycidylisobutyl—POSS (EP0418) ($C_{34}H_{74}O_{14}Si_8$) (Figure 1) was obtained from Hybrid Plastics™.

METHODS

Nanocomposite Manufacturing

The epoxy resin (DGEBA) was prepared based on the equivalents of the reactive groups (eq kg^{-1}) using cycloaliphatic amine as a curing agent. A molar ratio of 1/1 between the epoxy and amine groups was maintained. To obtain the nanocomposites, 1, 5, and 10% by weight (wt %) of glycidylisobutyl—POSS was added from a pre-mix to the epoxy resin using Sonics sonication equipment (VCX 750) operated at 225 W for 20 min. The resin curing was performed at a temperature of 25°C ± 3°C for 24 h. After curing, the samples were post-cured in an oven under a vacuum (300 mmHg) for 24 h at 120°C.

Sample Characterization

An RMC Power Tome XL ultramicrotome, equipped with a diamond knife, was used to cut the samples to a thickness of 50 nm at a speed of 0.3 mm s^{-1} and was done at room temperature. The sections were collected on copper grids (300 mesh) and analyzed by transmission electron microscopy (TEM). The thermal-mechanical analysis (TMA) was performed in aTMA-60 (Shimadzu) at 10°C min^{-1}witha load of 5N between 25 and 140°C in a nitrogen atmosphere (50 mL min^{-1}). The viscoelastic properties were characterized with a Q800 AT DMA instrument in a single-cantilever clamp using rectangular specimens measuring 35 × 10 × 2 mm^3. The sweep experiments were carried out at glass transition temperatures within the range of 40 to 120°C. The frequency was varied from 100 to 0.1 Hz at a rate of 10 points per decade at intervals of 3°C after temperature equilibration, and the resulting isothermal curves were analyzed using the Williams–Landel–Ferry (WLF) equation.[13] The parameters calculated in this study were directly related to the WLF and Vogel–Fulcher–Tumman (VTF) equivalence, as previously discussed.[14,15] The relaxation ($H(\tau)$) and retardation ($L(\tau)$) spectra were determined using nonlinear regularization (NLREG) software.[6,16,17]

RESULTS AND DISCUSSION

Morphology and Microstructure

Figure 2 shows the nanoparticle dispersion for the various POSS contents. The addition of 1% POSS revealed the presence of agglomerated cages on the surface analyzed. Furthermore, the presence of spheres with diameters of ≈15 nm was detected close to the agglomerates. For the samples containing 5 and 10% POSS, it was observed that the distribution of the sphere sizes predominately featured diameters of ~15 and 7 nm, as illustrated by the images (b) and (c), respectively. This predominance was observed in a series of analyzes. The dispersion process, as observed using the mentioned sonication method, occurs before the cure process. After the requisite exposure time for dispersion has elapsed, the solution is prepared for the cure process. Because the POSS is a hybrid structure, agglomeration may be due to the differences of surface energy of the cages (that have inorganic character) and the resin (organic character). Alternatively, considering that the major class of nanoparticles generally shows domains with nanoscale dimensions in only one dimension, as is the case with clays[18] and graphite,[19] the presence of these homogeneously distributed spheres with diameters in the range of 7–15 nm is indicative of expressive dispersion. In fact, these sphere sizes were expected for this type of system, which uses monofunctional POSS.[20–22] As demonstrated by Deng et al.,[20,21] the POSS cages can assumes a characteristic of amphiphilic structure. This characteristic is dependent on the organic groups present at the vertices of the cage and occurs because the cages (core structure) have an inorganic character that results in the cages being closer together to minimize their surface energy.

Figure 3 illustrates the relationship between the POSS shape and its physical and chemical interactions with the epoxy resin. At the lowest POSS content, the approximation image indicated that there was cage agglomeration. When the sonication was applied, it was noted that the ultrasonic irradiation promoted a separation of the cages. Immediately after sonication, the cage separation began to shrink in order to minimize the interfacial tension. As with the case of the glycidyl isobutyl—POSS, which is a monofunctional cage, the formation of micelles occurs due to the amphiphilic character[20–23] represented by the agglomeration of the inorganic portion (core cage) and the organic groups on the periphery of the formed spheres.

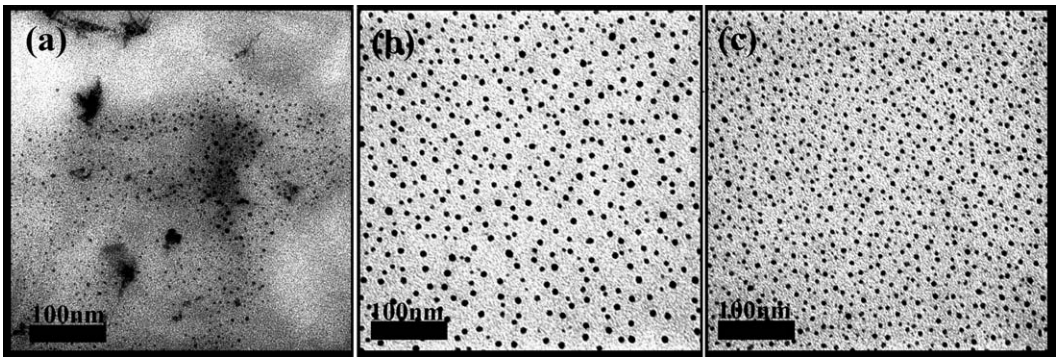

Figure 2. TEM images showed the dispersion of 1, 5, and 10% of POSS corresponding to (a), (b) and (c) respectively.

This interfacial tension resulted from differences between the chemical characteristics of the nanocage, which was formed by the inorganic fraction, and the organic substituent bonded in the vertices of the cage.[22] This type of morphology has been suggested as the core-shell formation.[23] Despite the breakage of clusters resulting from cavitations generated by the sonication process, the 1% POSS sample displayed agglomerates, whereas the 5 and 10% POSS samples presented fine dispersions. This increase of dispersion may be dependent of the increment of mass fraction (1, 5 and 10%). However, the observation that finer spheres were found for the 10% sample compared to the 5% sample may be due to the additional quantity of POSS (double) having generated spatial restrictions, which may have led to faster formation of micelles by the higher concentration of cages in the solution.

Dynamic-Mechanic Analysis (DMA)

Figures 4 and 5 illustrate the storage modulus (E') and tan δ curves. The glass transition ranged between 45 and 120°C in the samples. The vitreous (below $\approx$ 45°C) and elastomeric ($\approx$ 120°C) plateausdid not show significant changes with the addition of POSS. However, a change of slope in the modulus decrease was observed near the glass transition, mainly for samples containing 1 and 5% POSS. Furthermore, upon comparing tan δ curves to those of the DGEBA, it was found that the two maxima representing molecular mobility were observed for 1 and 5% POSS samples, whereas the behavior for the 10% POSS sample was similar to that of the DGEBA resin. The glass transition temperatures (T_g), measured from the tan δ curve, was 76°C for the DGEBA. Two maximum temperature peaks (67 and 93°C) and (70 and 94°C) were observed for the 1 and 5% POSS samples, respectively, as shown in Table I. For 10%, the T_g was 76°C.

It was possible to relate changes in T_g to the POSS dispersion and spatial distribution effects as a result of the POSS being able to form chemical bonds with the epoxy resin during the reticulation process.[3] The heterogeneity, which is indicated by the presence of the double peaks in the tan δ curves, may have resulted from the size domains of POSS in its agglomerated form at 1%, and this effect gradually diminished with an increase in nanocage concentration (5–10%), as the sphere size decreased, which resulted in the two peaks' morphing into one peak. Furthermore, for the 10% POSS sample, the more homogeneous distribution in its molecular mobility may be due to fine dispersion having reached a critical particle diameter that made it unable to cause perturbations in the crosslinking. The increase in T_g, mainly for 5 and 10% POSS samples, was correlated with an increase in the homogeneous dispersion, as shown in the TEM images.

In addition to T_g, the tridimensional network had sufficient thermal energy to overcome the potential barrier associated with a Van der Waals interaction. The chains underwent a short change in conformation through segmental cooperative motions, but the reticulations prevented any flow. A peculiar state of matter exists in this fundamental condition that displays liquid and elastic solid properties simultaneously (known as the viscoelastic behavior).[8] Using this concept, it is possible to estimate the crosslinking density (υ) and the number of structural

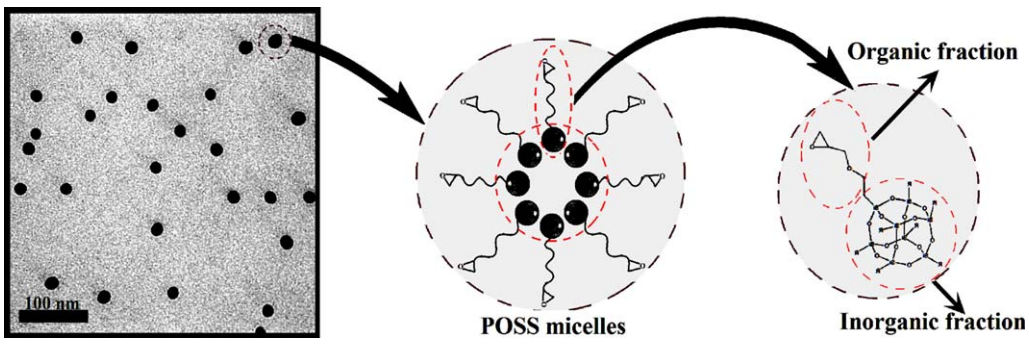

Figure 3. Schematic illustration comparing the formation of POSS micelles formed by nanocages at higher concentrations. [Color figure can be viewed in the online issue, which is available at wileyonlinelibrary.com.]

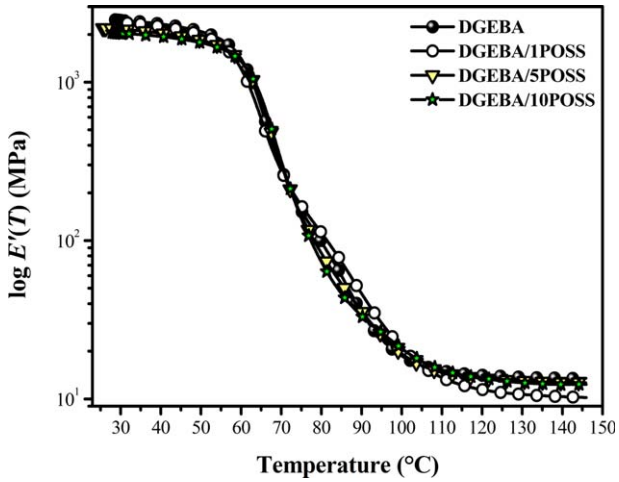

Figure 4. Storage modulus (E' (T)) as a function of the temperature for the epoxy resins and their nanocomposites. [Color figure can be viewed in the online issue, which is available at wileyonlinelibrary.com.]

units between crosslinks (υ_e) by using the rubber elasticity theory and considering the phantom networks[1,5,10] described by Eqs. (1) and (2)[5,9]

$$E_r = 3\varphi\upsilon RT \quad (1)$$

$$\upsilon_e = \frac{\rho}{M_w \upsilon} \quad (2)$$

where ϕ is the front factor that accounts for every factor distinguishing thermosetting from ideal rubber (*e.g.*, the short length of the elastic chains), υ_e is the concentration of elastic chains (mol cm^{-3}), R is the gas constant, T is the absolute temperature, ρ is the density, E_r is the modulus in the elastomeric plateau and M_w is the molecular weight of the structural unit. The value of ϕ is obtained from the behavior of the networks; however, a value of $\phi = 1$ can be used as an adequate order of magnitude prediction.[5] The results are illustrated in Table I.

At 140°C in the elastomeric region, the modulus decreased mainly for 1% POSS, and the values for those containing 5 and 10% POSS approached that of the resin. For 1% POSS, the presence of agglomerates may have caused more perturbations in the crosslinking network than for 5 and 10%. These perturbations maybe considered as formation of regions with varying crosslink densities and as clusters that created interfaces within the microstructure. These imperfections yielded discontinuities in the cooperative motion and are thus associated with the observed decreases in crosslink density. Alternatively, due to the bonds between the agglomerated particles with the DGEBA, the increase in υ_e maybe explained by an increase in the extent of percolation in the network crosslink. When the higher concentration of POSS was added, the dispersion and shape tended to minimize the fluctuations in the three-dimensional network, and as observed, the values of υ and υ_e approached that of the resin. Furthermore, with these physical changes in the network, the addition of POSS and the cluster formation showed a reinforcement effect on the increases in T_g, and its response was dependent on the shape of the nanoparticles and level of dispersion. Figure 6 illustrates the isothermal curves obtained within the frequency (ω) range of 0.1–100 Hz for the epoxy resin. All curves showed the same behavior, and the DGEBA resin was used to represent the construction of the master curves. A sweep experiment was carried at different temperatures and using T_g (Table I) as the reference temperature, with the parts of E' shifted to form the master curves. An average value of T_g (79°C) was used for 1 and 5% POSS loadings and was determined by convolution of the two peaks for each sample (Figure 5). Moreover, the WLF parameters are obtained at temperatures above the T_g ($\approx$10°C $> T_g$), where the free volume is considered constant.[24] The fits for determining C_1 and C_2 constants were performed with a confidence interval of 95%, with a margin of error <0.05% and coefficient of determination (r^2) higher than 0.998 for all samples. The $E'(\omega)$ master curves are shown in Figure 7.

At lower ωvalues, the relaxation times were larger and the chains had time to reach an equilibrium state of conformational motion. The increase in ω caused the molecular relaxation to decrease, and differences in structural cooperativity were noted. The addition of POSS yielded a decrease in the slope of $E'(\omega)$ and was most pronounced for 1% POSS loading. The sharp drop in the modulus is attributed as a consequence of interruption to cooperativity segmental motion.[6] This drop in the gradient, in combination with a decrease in υ and an increase in υ_e, suggested that the longer relaxation process could be attributed to the larger distance between the crosslinking points.

By considering the shift factor (a_T), which was taken when the master curves were shifted, or the shift of each modulus fraction on the ω axis, it was possible to determine the constants C_1 and C_2 described by William–Landel–Ferry (WLF)[13] and represented in the eq. (3). Using these constants, it was possible to determine the free volume (f_g), expansion thermal coefficient (α_f) and activation energy (ΔH_s) in T_g described by eqs. (4–6), respectively,[24]

$$\log a_T = \log[\tau(T)/\tau(T^*)] = C_1(T - T^*)/[T - (T^* - C_2)] \quad (3)$$

$$f_g = \frac{B}{2.303 \cdot C_1^g} \quad (4)$$

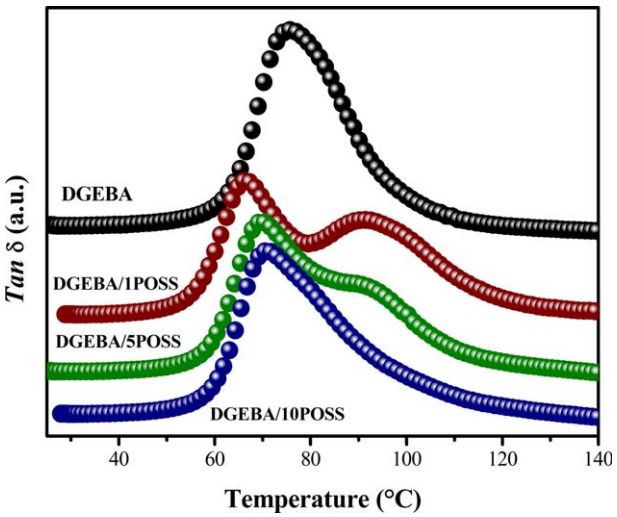

Figure 5. Tan δ curves as a function of the temperature to the samples studied. [Color figure can be viewed in the online issue, which is available at wileyonlinelibrary.com.]

Table I. Results Obtained by DMA and Estimated by the Phantom Model

Parameters	DGEBA	DGEBA/1 POSS	DGEBA/5 POSS	DGEBA/10POSS
T_g (°C)	76	67/93	70/94	76
$\rho_{(25°C)}$ (g cm^{-3})	1.083	1.081	1.080	1.078
$E'_{(140°C)}$ (MPa)	13.5	10.3	12.7	12.3
$\rho_{(140°C)}$ (g cm^{-3})	1.005	1.001	1.001	0.998
υ_e (10^{3}mol cm^{-3})	7.7	11.0	8.3	8.5
υ (mol g^{-1})	1.5 x 10^{-3}	1.2 x 10^{-3}	1.4 x 10^{-3}	1.4 x 10^{-3}

$$\alpha_f = \frac{B}{2.303 \cdot C_1^g \cdot C_2^g} \quad (5)$$

$$\Delta H_\alpha = \frac{2.303RC_1^0C_2^0T^2}{(C_2^0+T-T^*)^2} \; or \; \Delta H_\alpha = \left[\frac{2.303RC_1^0T^2}{C_2^0}\right]_{T=T^*} \quad (6)$$

where τ is the relaxation time at a temperature T, $\tau(T^*)$ is the relaxation time at a reference temperature (usually the reference temperature (T_g)) within the measurement range and C_1 and C_2 are the WLF constants.[14,25] C_1 is a constant that relates the phonon relaxation time with a relaxation time in T_g (100 s), while C_2 is related to the strength parameter of the strong/fragile liquids classification.[26] α_f is a parameter obtained by considering f_g and the structural fragility of the material, and even omitted effective values are a good estimation with which to compare behaviors between samples. However, the thermal expansion coefficient (α^*) at T_g was determined using TMA analysis, and these results are shown in Table II.

The addition of POSS had a tendency to reduce ΔH_α. On the one hand, thisreductioncould be attributed to the volume of nanocages, which resulted in decreases in intermolecular interaction that facilitated the molecular rearrangement of the three-dimensional network of the epoxy resin.[6] On the other hand, the reduction of the intermolecular forces may have been associated with molecular mobility, and in this case, the more obvious expected response would have been a reduction in T_g. However, as previously shown, the lowest activation energy was not necessarily associated with a lower T_g or shorter relaxation times.[1,5,6] The incorporation of POSS increased the total energy required to move chain segments along the three-dimensional network through the relationship with the percolation extension, even at the lower values of υ, which may have occurred because the larger extension was associated with the interconnections between the nodular interfaces, correlated with the fluctuations in the crosslinking. Thus, the increase in T_g was attributed to these interconnections (an attribution corroborated by the increased υ_e), and the reduction in ΔH_α as a consequence of the increase in free volume and reduction in the intermolecular forces between chains.[6]

The addition of POSS decreased α_f and α^* and was a relevant result because thermal expansion is undesirable in applications such as electronic devices. Moreover, the POSS could also promote decreases in thermal conductivity by increasing the distance between chains,[27] characteristics that have increased the interest in their electronic application. The decrease of α_f and α^* was also associated with the increase in percolation of the three-dimensional network, which restricted the motion of the chains.

Table II also shows the parameters obtained from the interrelationships of the WLF and Vogel–Fulcher–Tammann (VFT)

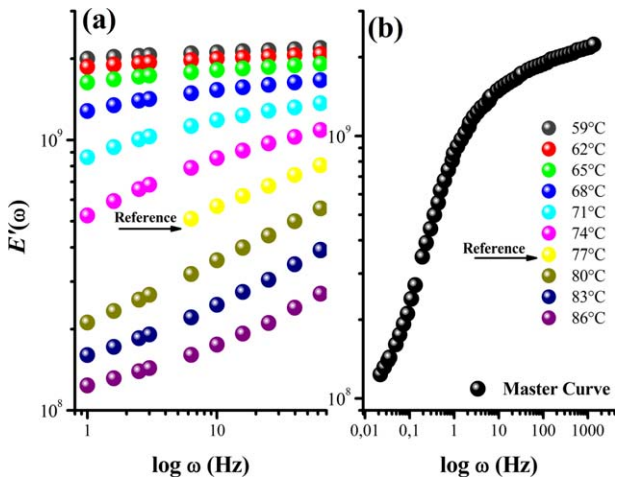

Figure 6. Fragments of the $E'(\omega)$, (a), obtained by frequency sweep at different isothermal temperatures and the shifts for the building the master curve, (b), using the T_g as reference. [Color figure can be viewed in the online issue, which is available at wileyonlinelibrary.com.]

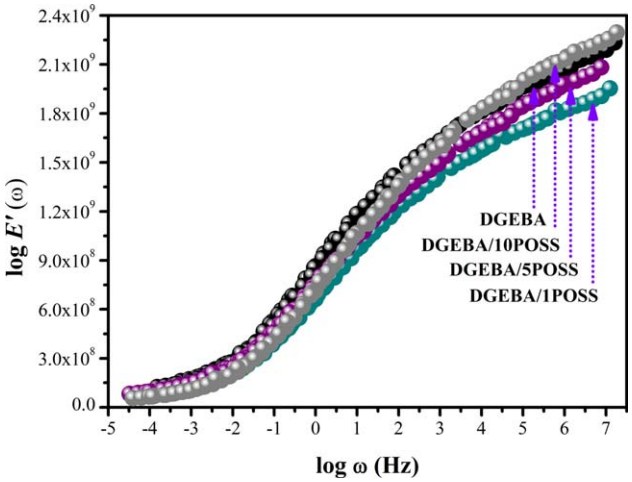

Figure 7. Master curves of the storage modulus ($E'(\omega)$) as a function of the frequency for the epoxy resins and their nanocomposites. [Color figure can be viewed in the online issue, which is available at wileyonlinelibrary.com.]

Table II. Parameters of the Phantom Model and the Equivalence Between WLF and VFT Equations

Parameters	DGEBA	DGEBA/1POSS	DGEBA/5POSS	DGEBA/10POSS
C_1	16.8	18.8	17.4	16.0
C_2 (K)	60.1	71.4	66.5	63.5
r^2	−0.9986	−0.9991	−0.9989	−0.9995
Error C_1/C_2 fit	±0.98	±1.42	±1.21	±1.05
ΔH_α (kJ mol^{-1})	475.3	470.9	457.4	416.7
f_g	0.0259	0.0231	0.0250	0.0271
α_f (10^{-4}K^{-1})	4.31	3.23	2.50	2.71
α^a (10^{-7}K^{-1})	17.83	16.81	5.05	5.47
B	2325	3091	2664	2339
T_0 (K)	281	268	276	280
Z(T)	6	-	–	5
M	21.5	21.06	21.7	20.9

[a] Thermal expansion coefficient measured by TMA at the T_g.

equations.[14,15] The WLF equation follows the Arrhenius dependence, while the VFT, as shown in eq. (7), describes the deviations from the Arrhenius temperature dependence.

$$\tau = \tau_0 \exp\left(B/(T - T_0)\right) \quad (7)$$

B and T_0 in the VFT equation define the relaxation activation energy and ideal glass transition derived from the Adams–Gibbs equation, respectively, and can be defined as (B(K) = C$_1$.C$_2$.ln10) and ($T_0 = T_g$ -C_2).[26] The addition of POSS mainly increased B at 1% content and decreased B at 5 and 10% content, the latter approaching the behavior of the DGEBA resin. Because B is correlated with the energetic barrier of molecular relaxation, this result was corroborated by the υ parameter. The higher crosslink density required more energy to undergo the energetic barrier of relaxation. However, the changes in crosslink density, as discussed above, can occur due to discontinuities in cooperative motion, and these micro structural imperfections can be indirectly correlated with cooperative rearrangement regions (CRR).[7] These CRR are described as subsystems that can undergo rearrangements by thermal fluctuations and are directly associated with the potential energy of hyper surfaces.[11,28,29] The greater the imperfections in the microstructure are, the higher the quantity of interfaces, which are described as CRR.[6,7] The fluctuations in the potential energy complicate the emergence of a glass transition in a defined temperature range, and for this reason, the values are dependent on the experimental measurement conditions because the CRR can be randomly activated during thermal fluctuations. However, the experimental defined transition is not necessary to understand the metastable state in the glass transition, and the evaluation of T_g can be used to evaluate the modifications to the material from a structural interface point of view.[30] Accordingly, T_0 represents the ideal glass transition temperature when the material is dependent on a minimum number of microstructural imperfections and rearrangement effects.[10,12] As seen in this experiment, T_0 showed the same tendency as B, and the difference between T_g (Table I) and T_0 increased with 1% POSS content and was subsequently minimized at 5 and 10% POSS content. With this two temperatures, the average size of the CRR (Z(T)) can be estimated using eq. (8).[6]

$$Z(T) = \frac{T_g}{T_g - T_0} \quad (8)$$

The value of $Z(T)$ for 10% POSS was lower with the DGEBA resin. Calculation was not possible for 1 and 5% POSS loading due to the two maximums of T_g (Figure 5). The decrease in $Z(T)$ suggested that more interfaces led to a more fragile material (in terms of molecular rearrangements), and so a reduction in T_g should have been observed. However, POSS is a functional nanoparticle, and the formation of micelles is an important factor that increases the resin percolation, even in the presence of clusters. This characteristic was corroborated by the increase of υ_e (Table I).

The fragility concept presented by Angell in 1985[25] is a method of classifying materials as strong or fragile in terms of their susceptibility to molecular rearrangement. In other words, when the material displays Arrhenius behavior during cooling, it is considered strong, and if it does not display Arrhenius behavior (i.e., it displays non-Arrhenius behavior), it is considered fragile. This condition can be observed through the measurement of different properties, such as calorific capacity (C_p), enthalpy (ΔH) and entropy (ΔS) variations and relaxation time (τ) and viscosity (η), as a function of temperature. The fragility index (m) characterizes the apparent activation energy of structural relaxation in T_g normalized by the maximum value of T_g.[31] The index values range between two limits, $m = 16$ (strong) and $m = 250$ (fragile).[32] For example, a strong material with an m value close to 16 is associated with crystalline and thermosetting materials due to either the oriented molecular arrangement or the crosslink network, respectively, which complicates the rearrangement of such structures. An m value close to 200 is associated with a fragile structure, such as the glass-forming liquids.[33]

The addition of POSS yields no significant variation in m values; however, as the fragility index is a method of correlating changes in microstructure with entropic and energetic factors. A

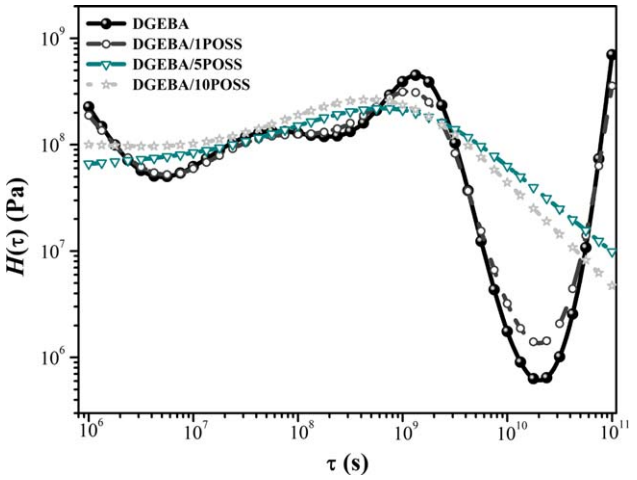

Figure 8. Relaxation ($H(\tau)$) spectra obtained by the nonlinear regularization (NLREG) method. [Color figure can be viewed in the online issue, which is available at wileyonlinelibrary.com.]

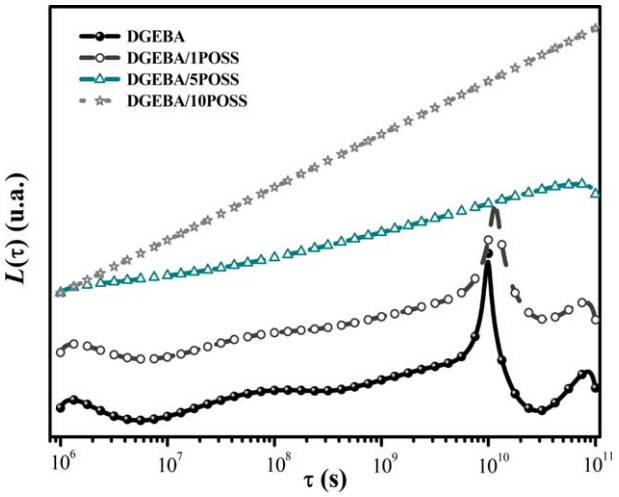

Figure 9. Retardation ($L(\tau)$) spectra obtained by the nonlinear regularization (NLREG) method. [Color figure can be viewed in the online issue, which is available at wileyonlinelibrary.com.]

lack of variation of m compared with a decrease in Z(T) indicates that the formation of DGEBA/POSS clusters is favorable because the bonds in the peripheral regions of the clusters maintain the percolation of the network and cause a reinforcement effect on T_g in the DGEBA. To evaluate the dependence of the percolation on relaxation times, Figures 8 and 9 show the relaxation ($H(\tau)$) and retardation ($L(\tau)$) time spectra obtained using eqs. (9) and (10), respectively,[24]

$$H(\tau)=\frac{L(\tau)}{\left[J_g+\int_{-\infty}^{\infty}\frac{L(\tau)}{(1-\tau)/\tau}d\ln\tau-\frac{\tau}{\eta_0}\right]^2+\pi^2L(\tau)^2} \quad (9)$$

$$L(\tau)=\frac{H(\tau)}{\left[G_\theta-\int_{-\infty}^{\infty}\frac{H(\tau)}{\tau/(\tau-1)}d\ln\tau\right]^2+\pi^2H(\tau)^2} \quad (10)$$

where G_θ and J_g are the modulus and compliance of equilibrium, respectively, and τ is the relaxation time. The $H(\tau)$ and $L(\tau)$ spectra were calculated based on the master curves (storage (E') and loss (E'') moduli) obtained from a time–temperature superposition of the DMA.[6] The $H(\tau)$ results were obtained from the sum of the Maxwell infinite elements, which describe the mechanical behavior on the elastic portion of a polymer.[6,16] The estimation of the retardation spectrum was performed through the interrelations of the spectra described by Ferry and from results on Voigt's sum of the infinite elements, which control the entire viscous portion of the polymer.[19] From the DGEBA, two relaxation distributions were evident, with in which the maximum peakswere at $H(\tau) \approx 4\times10^7$ s and 2×10^9 s and $L(\tau) \approx 6\times10^7$ sand 10^{10} s, respectively. For each relaxation time (correlated with the elastic portion), there existed a retardation time (viscous portion), illustrated in Figure 9, which provides a delayed response in relation to the relaxation time.

The first relaxation phenomenon mentioned was correlated with the vibration and conformation of the epoxy resin backbone, whereas the second relaxation phenomenon was related to movement at the interface between the domains of the crosslinked regions (nodular domains) or the characteristic domains that resulted from inhomogeneous epoxy resin curing. Both relaxation stages were compared with the literature and corresponded to the same time scale range.[6]

Two relaxation stages were identified with the addition of 1% POSS, but a slight reduction occurred in the peak intensity. With 5 and 10% POSS content, a single large peak was identified along the entire DGEBA relaxation range. The appearance of a single large distribution indicated that the two stages overlapped due to the interconnections of the nodules with the POSS micelles. This result also corroborated the observed increase in T_g and the reduction of α_f and α^* because the microstructure did not present an interfacial degree of freedom related to nodule rearrangement. Because of the higher cooperativity in the relaxation or mobility, the viscous portions illustrated by $L(\tau)$ were restricted and the retardation response was not observed at this time scale. The molecular interactivity in the presence of the POSS micelles favored elastic behavior and corroborated the observed increases in T_g, the reduction in thermal expansion and the lower activation energy without decreasing the structural fragility.

CONCLUSIONS

An epoxy containing monofuctional glycidil isobutyl—POSS was prepared and the relationship between the dispersion characteristics and the glass transition state was evaluated. With the addition of 5 and 10% POSS, there was greater dispersion in a spherical shape correlate with the amphiphilic character of the hybrid cages.

The phantom model showed for 5 and 10% POSS loading an increase in the number of structural units between crosslinks, which suggested higher percolation of the microstructure due to the micelles' favoring the higher interconnection. The addition of POSS decreased the activation energy of mobility and relaxation due to the volume of the POSS nanocages reducing the interaction forces between the chains. The nanostructure

systems showed lower thermal expansion due to the higher cooperativity of the interconnected microstructure. The DGEBA resin showed two stages of relaxation distribution, whereas with the addition of POSS, the relaxation process became more homogeneous due increased network percolation. These characteristics were favorable because of the reinforcement effect on T_g, and the reduction in thermal expansion suggested that the material possessed greater percolation without an increase in structural fragility.

ACKNOWLEDGMENTS

The authors gratefully acknowledge UCS, CAPES, and CNPq for providing scholarships and financial support.

REFERENCES

1. Pellice, S. A.; Fasce, D. P.; Williams, R. J. J. *J. Polym. Sci. B Polym. Phys.* **2003**, *41*, 1451.
2. Zhang, T.; Lee, S.; Yoonesi, M.; Liang, K.; Pittman, C. U. *Polymer* **2006**, *47*, 2984.
3. Strachota, A.; Whelan, P.; Kriz, J.; Brus, J.; Urbanova, M.; Slouf, M.; Matejka, L. *Polymer* **2007**, *48*, 3041.
4. Zucchi, I. A.; Galante, M. J.; Williams, R. J. *J. Eur. Polym. J.* **2009**, *45*, 325.
5. Pistor, V.; Ornaghi, F. G.; Ornaghi, J. R. H. L.; Zattera, A. *J. Mater. Sci. Eng. A* **2012**, *532*, 339.
6. Pistor, V.; Barbosa, L. G.; Soares, B. G.; Mauler, R. S. *Polymer* **2012**, *53*, 5798.
7. Pistor, V.; Soares, B. G.; Mauler, R. S. *Polymer* **2013**, *54*, 2292.
8. Pascault, H. S.; Verdu, J.; Williams, R. J. J. Thermosetting Polymers; Marcel Dekker: New York, **2002**.
9. Vanlandingham, M. R.; Eduljee, R. F.; Gillespie, J. R. J. W. *J. Appl. Polym. Sci.* **1999**, *71*, 699.
10. Qazvini, N. T.; Mohammadi, N. *Polymer* **2005**, *46*, 9088.
11. Angell, C. A. *Phys. D* **1997**, *107*, 122.
12. Adam, G.; Gibbs, J. H. *J. Chem. Phys.* **1965**, *43*, 139.
13. Williams, L. M.; Landel, R. F.; Ferry, J. D. *J. Am. Chem. Soc.* **1955**, *77*, 3701.
14. Kovacs, A. *J. Adv. Polym. Sci.* **1964**, *3*, 394.
15. Angell, C. A. *Polymer* **1997**, *38*, 6261.
16. Roths, T.; Marth, M.; Weese, J.; Honerkamp, J. *Comp. Phys. Commun.* **2001**, *139*, 279.
17. Weese, J. *Comp. Phys. Commun.* **1993**, *77*, 429.
18. Ray, S. S.; Okamoto, M. *Prog. Polym. Sci.* **2003**, *28*, 1539.
19. Yasmin, A.; Daniel, Y. M. *Polymer* **2004**, *45*, 8211.
20. Deng, J.; Polidan, J. T.; Hottle, J. R.; Farmer-Creely, C. E.; Viers, B. D.; Esker, A. R. *J. Am. Chem. Soc.* **2002**, *124*, 15194.
21. Deng, J.; Hottle, J. R.; Polidan, J. T.; Kim, H.-J.; Farmer-Creely, C. E.; Viers, B. D.; Esker, A. R. *Langmuir* **2004**, *20*, 109.
22. Zeng, K.; Zheng, S. *J. Phys. Chem. B* **2007**, *111*, 13919.
23. Zhang, W.; Müller, A. H. E. *Prog. Polym. Sci.* **2013**, *38*, 1121.
24. Ferry, J. D. Viscoelastic Properties of Polymers, 3rd ed; Wiley: New York, **1980**.
25. Angell, C. A. *J. Non-Cryst. Solids* **1985**, *73*, 1.
26. Ornaghi, J. R. H. L.; Pistor, V.; Zattera, A. J. *J. Non-Cryst. Solids* **2012**, *358*, 427.
27. Zhang, Z.; Gu, A.; Liang, G.; Ren, P.; Xie, J.; Wang, X. *Polym. Degrad. Stabil.* **2007**, *92*, 1986.
28. Solunov, C. A. *Eur. Polym. J.* **1999**, *35*, 1543.
29. Saiter, J. M.; Dobircau, L.; Saiah, R.; Sreekumar, P. A.; Galandon, A.; Gattin, R.; Leblanc, N.; Adhikari, R. *Phys. B* **2010**, *405*, 900.
30. Simon, S. L.; Mckenna, G. B. *J. Non-Crystalline Solids* **2009**, *355*, 672.
31. Sokolov, A. P.; Novikov, V. N.; Ding, Y. *J. Phys. Condens. Matter* **2007**, *19*, 1.
32. Delbreilh, L.; Bernès, A.; Lacabanne, C.; Grenet, J.; Saiter, J.-M. *Mater. Lett.* **2005**, *59*, 2881.
33. Angell, C. A. *J. Phys. Chem.* **1993**, *97*, 6339.